Große-Kreul *et al. EPJ Techniques and Instrumentation* (2016) 3:6
DOI 10.1140/epjti/s40485-016-0034-1

EPJ Techniques and Instrumentation
a SpringerOpen Journal

RESEARCH ARTICLE Open Access

Methods of gas purification and effect on the ion composition in an RF atmospheric pressure plasma jet investigated by mass spectrometry

Simon Große-Kreul, Simon Hübner, Simon Schneider, Achim von Keudell* and Jan Benedikt

*Correspondence:
Achim.vonKeudell@rub.de
Institute for Experimental Physics II, Ruhr-Universität Bochum, 44780 Bochum, Germany

Abstract

The analysis of the ion chemistry of atmospheric pressure plasmas is essential to evaluate ionic reaction pathways during plasma-surface or plasma-analyte interactions. In this contribution, the ion chemistry of a radio-frequency atmospheric pressure plasma jet (μ-APPJ) operated in helium is investigated by mass spectrometry (MS). It is found, that the ion composition is extremely sensitive to impurities such as N_2, O_2 and H_2O. Without gas purification, protonated water cluster ions of the form $H^+(H_2O)_n$ are dominating downstream the positive ion mass spectrum. However, even after careful feed gas purification to the sub-ppm level using a molecular sieve trap and a liquid nitrogen trap as well as operation of the plasma in a controlled atmosphere, the positive ion mass spectrum is strongly influenced by residual trace gases. The observations support the idea that species with a low ionization energy serve as a major source of electrons in atmospheric pressure helium plasmas. Similarly, the neutral density of atomic nitrogen measured by MS in a He/N_2 mixture is varying up to a factor 3, demonstrating the significant influence of impurities on the neutral species chemistry as well.

Keywords: Ion mass spectrometry, Atmospheric pressure plasma, Gas purification

Introduction

A large variety of devices used for the generation of atmospheric pressure plasmas (APPs) has been developed in the past. The design, applied voltage waveform and used gas mixture vary strongly in dependence of the desired purpose [1]. A lot of different examples can be found in the literature varying from direct-current driven hollow cathode discharges [2] to dielectric barrier discharges [3] (driving voltage in the range of 1–20 kHz with peak-to-peak voltage of the order of several kV) to capacitively or inductively coupled radio-frequency APPs [4] (1–100 MHz, below 1 kV peak-to-peak voltage).

A significant effect of APPs on delicate surfaces can be observed using rather simple experimental setups. However, the involved complex physical and chemical processes have to be studied to understand and tune the desired effects. The list of possible applications is long, e.g. deposition of wear-resistant SiO_2 thin films [5–7], pre-treatment of

polymers before printing [8–10], sterilization/inactivation of medical tools and treatment of infectious chronic wounds [11, 12] to name only some of them.

It has been shown that APP generated ions can play a significant role in chemical processes relevant for the interaction of plasmas with living cells, e.g. inactivation of the bacterium 'Escherichia coli' [13, 14]. Moreover these ions are used for chemical ionization (mostly proton transfer reactions) used in analytical mass spectrometry [15]. A profound understanding by further investigation of the involved plasma-chemical reaction pathways, in particular of plasma-generated ions, is therefore necessary.

Mass spectrometry (MS) is a powerful tool for ion analysis of APPs. A detailed review about MS of APPs can be found in our recent article [16]. The ion chemistry in the afterglow of non-thermal plasmas at atmospheric pressure is dominated by the formation of cluster ions of the form $H^+(H_2O)_n$ due to the inherent presence of water. For example, water cluster ion formation plays an important role in the upper atmosphere, where the dimer ion $H^+(H_2O)_2$ is dominating the ion composition in the D region (60 km to 90 km altitude) of the ionosphere [17]. But also in the case of laboratory plasmas, the majority of detected ions of both polarities appear in the form of clusters as shown by numerous studies in the past [8, 18–23]. This observation is independent of the technical realization of a specific APP, of the applied voltage waveform and of the employed gas mixture. The high number of collisions during the sampling process and the permanent dipole moment of water favors the formation of such clusters. In analytical MS systems, especially in the case of proton transfer MS, the presence of water cluster ions is inevitable and must be taken into account [15]. However, in the case that the plasma chemistry itself is the focus of investigation, the formation of water clusters obscures the bulk plasma chemistry and valuable information is lost.

Many previous studies dealing with the analysis of the ion chemistry of APPs by MS were performed in a non-controlled atmosphere, i.e. the plasma sources were operated in ambient laboratory air. One exception is the study of Bruggeman et al. [18]. However, in that case water is admixed on purpose to an atmospheric pressure glow discharge leading to the expected formation of water cluster ions.

The significant effect of gas impurities on the plasma neutral chemistry could already be demonstrated by absorption spectroscopy showing a reduction of the lifetime of Helium metastables with increasing impurity concentration [24]. Similarly in APPs driven in argon gas, it was shown that water impurities change the reactive species composition and cell viability [25].

Summarizing, the investigation of ions in an APP source under clean and well-defined conditions is motivated mainly due to three reasons:

1. In some applications the plasma is in close proximity to the surface to be treated. Therefore, sampling of primary ions is required to identify and study relevant mechanisms during this direct plasma-surface interaction. It will be shown that reducing impurities is not only changing strongly the ion chemistry but that the neutral composition is influenced as well.
2. For chemical ionization in analytical MS systems it is crucial to determine which ion (which ionization potential) interacts with the analyte. The variation of the impurities at our APP helps to predict the best regimes to favour individual ionization channels.

3. The reduction in complexity of the involved neutral species allow us to simplify the system for successful numerical simulation of the plasma chemistry, i.e. to reduce the number of relevant reaction pathways. This helps to validate models as well as to gain insight into the core plasma chemistry rather than analyzing secondary products formed during the sampling process.

The above-mentioned points are addressed in this contribution by mass spectrometric investigation regarding the effect of feed gas purification and operation of the plasma source in a controlled atmosphere on the composition of ions sampled from a micro plasma jet operated in helium.

Experimental set-up and procedures

Atmospheric pressure ion mass spectrometry

The micro atmospheric pressure plasma jet (μ-APPJ) has been in the focus of many studies in the past and is described in great detail in [4, 26–30]. Here, a short description of the recent design will be given together with the operating procedure. The μ-APPJ is a planar version of the originally coaxial atmospheric pressure plasma jet first introduced by Selwyn et al. [31].

This planar jet consists of two stainless steel electrodes that are enclosed by windows made from quartz glass. A gas channel with a square cross section of 1 mm × 1 mm with a length of 30 mm is formed by the two electrodes and two glass plates. A special vacuum-compatible glue (Torr Seal®) is used for mechanical stability as well as for sealing the sandwich structure. By this it is ensured that no volatile compounds from solvents or the atmosphere are contaminating the gas. By applying a radio-frequency voltage with a standard value of $U_{rms} = 210\,\mathrm{V}$, a capacitively coupled plasma is ignited in He flowing at a standard flow rate of 1.4 slm between the two electrodes. Admixtures of reactive gases such as N_2 or O_2 (usually < 1 %) can be used.

A schematic diagram of the experimental setup used for ion sampling and analysis is shown in Fig. 1. The experimental setup consists of three sections. In the first section ions are generated by an atmospheric pressure plasma. The plasma is housed in a pre-chamber that consists of a cylinder made from borosilicate glass. This allows the sampling of the exhaust of the μ-APPJ in a controlled atmosphere. The ions from the plasma are sampled from the effluent through an orifice with a diameter of 20 μm into the first pumping stage ($p_1 \approx 10^{-4}\,\mathrm{mbar}$). Here the ions are extracted by a set of cylindrical electrostatic lenses (U_1, U_2, U_3 and U_4) as indicated in Fig. 1. By this, ions are focused into the second pumping stage ($p_2 \approx 10^{-7}\,\mathrm{mbar}$) that is housing a mass spectrometer with a built-in quadrupole mass analyzer (Hiden PSM) and a 'Bessel box' energy analyzer. All measurements shown here are performed at a fixed ion energy of about 0.25 eV. As shown in [16] the energy of the sampled ions depends on the ion mass. This inherent effect ('seeded beam effect') of the isentropic expansion of the gas from atmospheric pressure into vacuum, may result in an over- or underestimation of ratios of ion signals obtained from measurements performed at a fixed pass energy set in the energy analyzer. However, this effect does not change any relative trends measured at a given mass as function of some process parameter such as gas purity or distance from the plasma, which is the relevant factor for the study presented here.

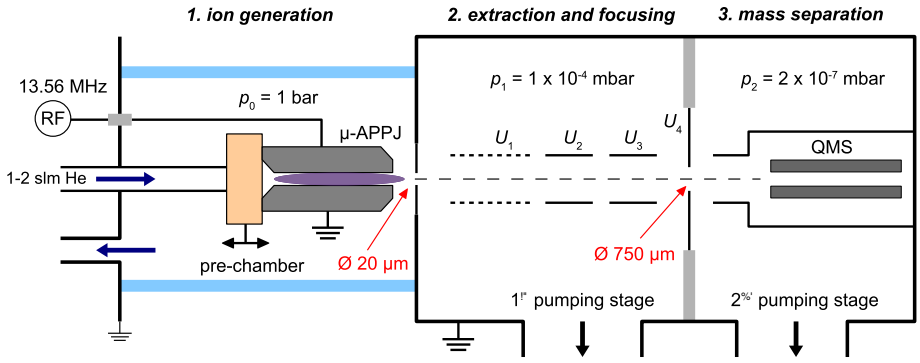

Fig. 1 Schematic diagram showing the feed gas preparation of the μ-APPJ. Mass flow controller (MFC) with different flow rates are used for supply of the feed gas which is purified using a molecular sieve trap (MC50, SAES Pure Gas, Inc.) and a liquid nitrogen trap

The plasma device is mounted on a linear stepper motor which can adjust the distance accurately even when the chamber is closed. Preliminary alignment in the other two dimensions is crucial and is performed by using adjustable mounting posts.

Control of gas purity

The plasma source is operated using Helium (5.0) with a purity of 99.999 % which means that impurities with a concentration of about 10 ppm are present in the plasma. According to the gas supplier the impurities are composed of 4 ppm N_2, 1 ppm O_2, 3 ppm H_2O and residual noble gases with a concentration smaller than 1 ppm such as Ar and Ne. Additional sources of impurities are small leaks in the feed gas lines and desorption from the inner walls of those. The final level of impurities reaching the plasma is therefore always slightly higher. The feed gas purity is essentially depending on the type of gas connection, i.e. using polymer or a stainless steel tubing. In addition the feed gas may be purified by means of a molecular sieve trap and a liquid nitrogen trap as shown in Fig. 2.

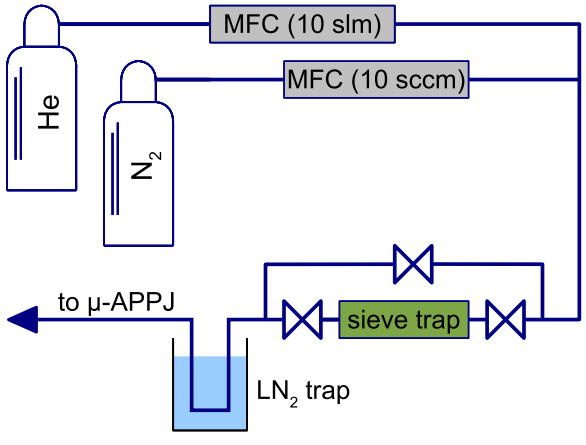

Fig. 2 Schematic diagram showing the experimental setup used for the extraction of ions from atmospheric pressure plasmas. The atmospheric pressure plasma jet is placed in a pre-chamber in front of the orifice at a variable distance

Effect of gas purity on the plasma chemistry

Effect of gas tubing material

The material chosen for the tubing of the feed gas line as a source of impurities has a strong influence on the ion chemistry in a helium-based plasma. The effect of impurities from the feed gas on the ion composition is illustrated by comparing mass spectra obtained from the μ-APPJ where the gas supply is connected by two different methods. In Fig. 3(a) a mass spectrum in units of mass per charge versus counts per second obtained from the μ-APPJ connected via a tube made from polyamide (PA) is shown. This is compared with a mass spectrum shown in Fig. 3(b) obtained under identical operating conditions but with a feed gas connection via a tube made from stainless steel. A significant difference between both spectra is clearly visible.

Water cluster ions of the form $H^+(H_2O)_n$ up to $n = 5$ are dominating the spectra although the jet is operated in a controlled atmosphere using helium (5.0) without additional admixture of reactive gases. The major difference between the two spectra shown in Fig. 3(a) and (b) is that in the case of the connection via the PA gas line only large water clusters $H^+(H_2O)_4$ and $H^+(H_2O)_5$ are observable while in the case of a gas line made from stainless steel smaller clusters with $n < 4$ are observable. In addition, the integrated ion signal is significantly lower indicating a lower ionization degree when a PA tube is used for feed gas transport.

The spectrum obtained from the plasma connected via PA-tubing is stable in time while the spectrum obtained from the plasma connected via stainless steel tubes changes during the first hour of operation which is shown in Fig. 3(c). The general tendency is that

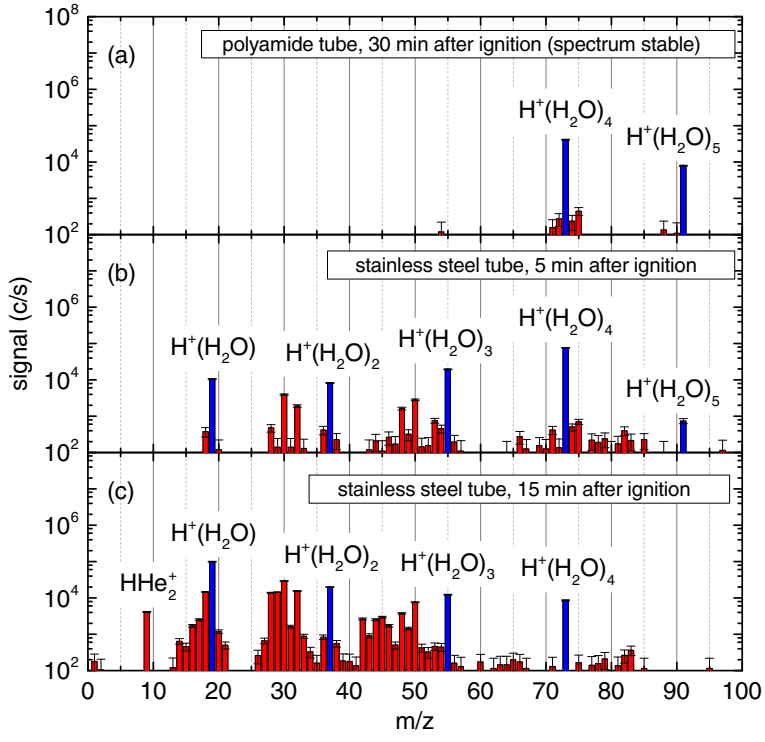

Fig. 3 Effect of Type of feed gas connection ((**a**) polyamide tube; (**b**) stainless steel 5 min After ignition; (**c**) stainless steel 15 min after ignition) on mass spectra obtained from the analysis of the μ-APPJ operated in a controlled atmosphere, no admixture of reactive gases, 2 mm distance to orifice

lower mass ions become more abundant with increasing operation time of the plasma. This observation is underlined in Fig. 4 where the signals of the first four water cluster ions are shown in dependence on the operation time of the plasma. The effect can be explained by a decreasing rate of water desorption from the tubes and electrodes resulting in a reduced probability for water cluster ion formation. Tubes made from PA have the advantage of being flexible and easy to mount which is tempting for the quick realization of an experimental setup. However, the flexibility of PA is based on the absorption of water. This water is continuously outgassing from the inner wall of the tube which results in contamination of the helium. Finally, water cluster ions are dominating the spectrum and reproducible operating conditions are not possible. The size of the clusters depends on the water concentration and residence time in the afterglow leading to the observation of heavy clusters when the feed gas line is made from PA. In case that the experimental setup requires to work with polymers, less permeable tubes made from PTFE, POM or Viton are a better choice.

However, even if the gas line is made from stainless steel, water cluster ions are still dominating the spectrum. Two reasons are suggested for this observation: (1) In the chain of charge transfer reactions among primary ions with neutral gas species the charge is generally transferred to the species with the lowest ionization energy. (2) Penning ionization through helium metastables plays an important role in the creation of ions in atmospheric pressure plasmas [27]. The He(2^3S) state carries an energy of 19.8 eV which allows it to readily ionize any other atomic or molecular species (except neon) with their typical ionization energies that are between 10 eV and 15 eV [32] within the bulk plasma of the jet. A similar amount of energy is also carried by He_2^* excimers, which have been

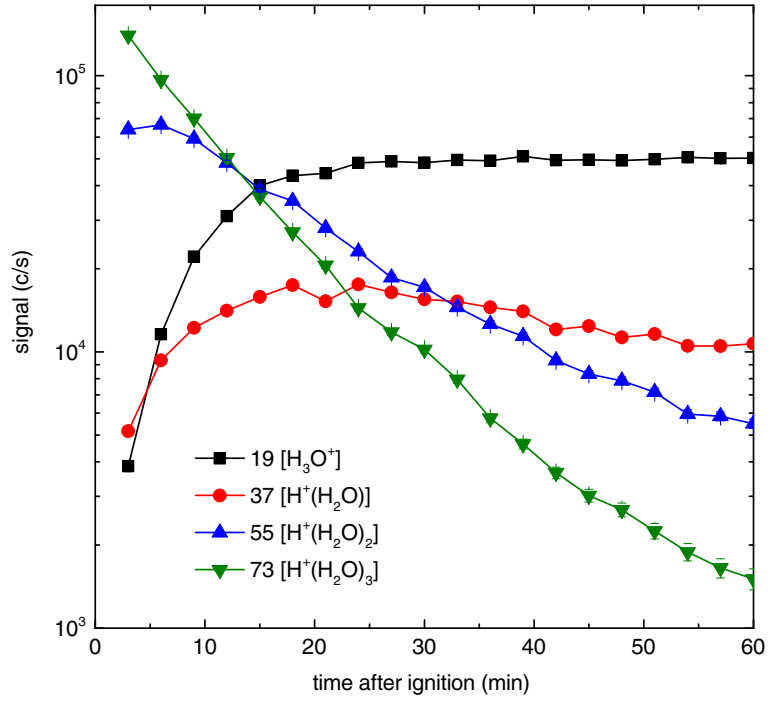

Fig. 4 Time-resolved water cluster ion signals after ignition of the μ-APPJ operated in pure helium connected via a tube made from stainless steel

observed from the same plasma source by vacuum-UV spectroscopy in our group [33]. Penning ionization of water molecules is followed by proton transfer. The terminal hydronium ion, similar to other terminal ions, can collect other neutral water molecules in an exothermic chain reaction:

$$\mathrm{He}(2^3\mathrm{S}) + \mathrm{H_2O} \rightarrow \mathrm{H_2O^+} + \mathrm{He}(1^1\mathrm{S}) + e^- \quad (1)$$

$$\mathrm{H_2O^+} + \mathrm{H_2O} \rightarrow \mathrm{H_3O^+} + \mathrm{OH} \quad (2)$$

$$\mathrm{H_3O^+} + n \cdot \mathrm{H_2O} \rightarrow \mathrm{H^+(H_2O)}_{n+1} \quad (3)$$

The error bars shown in Fig. 3 and following are based on random error of the counting unit in a specific single experiment. It should be noted that systematic issue with the reproducibility induce a much larger error bar of maybe 10 % of the value. However, that cannot be evaluated accurately since it depends strongly on the history of the plasma jet and vacuum chamber. The message of the presented measurements is not influenced (much) by the reproducibility because only qualitative conclusions are made.

Effect of feed gas connection and gas purification

The effect of the methods for gas purification illustrated in Fig. 2 are investigated by analyzing the ion composition of a μ-APPJ operated at a gas flow rate of 1.4 slm He and an admixture of 0.25 % N_2. The additional admixture of nitrogen as a reactive gas is necessary, since the plasma becomes unstable when the impurity concentration at a fixed generator power is changed in situ. The latter will be the case when the methods shown in Fig. 2 are applied. This underlines that molecular impurities with a low ionization energy are necessary as an electron source to sustain the plasma in the μ-APPJ operated in helium.

The effect of gas purification on the measured ion composition is shown as a time-resolved measurement in Fig. 5. The signals obtained from ions with highest abundance (H_3O^+, O_2^+, N_2^+ , N_3^+, N_4^+, NO^+) are monitored while switching on the gas purifier as well as the liquid nitrogen trap sequentially. The initial conditions at $t = 0$ correspond to the ion composition measured under operation of the jet in a controlled atmosphere after two hours of operation time.

At $t \approx 60$ s the path of the gas flow is switched by opening the valves in front and behind the gas purifier and closing the bypass valve. All observed signals show a significant response to the gas purification. The signals from pure nitrogen species N_x^+ increase by a factor of 3 to 4 while the signals from the oxygen containing species NO^+, O_2^+ and H_3O^+ are decreasing. In the case of NO^+ and O_2^+ the signals decrease only by 10 % and 25 %, respectively. In the case of H_3O^+ the signal reduction by a factor of 4 is much more distinct. Apparently the gas purifier that is based on chemical absorption of impurities is more effective for absorption of water than for absorption of oxygen.

Further purification of the gas is achieved by cooling a small section of the gas pipe with a length of $\sim$ 30 cm by passing the line through a dewar vessel filled with liquid nitrogen at $t \approx 180$ s. A significant reduction of the signal corresponding to H_3O^+ by two orders of magnitude is observed which is explained by condensation and freezing of water on the inner walls of the gas tube. The O_2^+ signal is reduced to around 50 %. The boiling temperature of liquid oxygen is 90 K which is above the boiling temperature of liquid nitrogen of 77 K. This can result in the observed reduction of the O_2^+ signal. Also

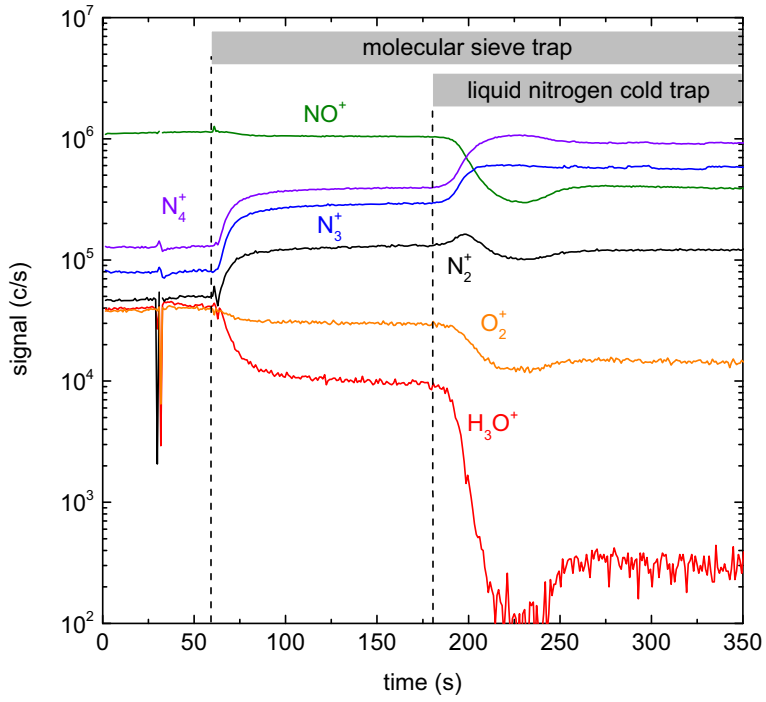

Fig. 5 Time-resolved measurement showing the significant effect of two purification methods (molecular sieve trap at $t = 60$ s and liquid nitrogen trap at $t = 180$ s) applied to the feed gas line of the μ-APPJ operated at a gas flow rate of 1.4 slm He and an admixture of 0.25 % N_2. The admixture of nitrogen is mandatory for stable operating conditions

for the latter signal the liquid nitrogen trap is more effective than the gas purifier. Similarly a signal drop of NO^+ of approximately 50 % is observed.

The nitrogen species do not react identically to the cooling of the gas line. While the signals of N_3^+ and N_4^+ increase each by about a factor of 2, the signal of N_2^+ is more or less constant when cooling the gas line. A possible explanation for that behaviour could follow the reasoning: The amount of clustering and charge transfer partners for N_2^+ is drastically reduced (H_2O and NO) such that N_2^+ should increase upon purification of the gas. A small hump can be found at $t = 200$ s in Fig. 5, however, the extra density seems to be captured by attachment reactions to form larger N_x^+ ions. For the increase of N_3^+ also the lower abundance of oxygen-based scavengers for atomic nitrogen or the reduced quenching of excited nitrogen states can cause the increase upon purification.

Temperature measurements using a thermocouple in the effluent of the jet reveal that the gas reaches room temperature within the gas line after the liquid nitrogen trap. Therefore, the observed signal reduction is solely due to purification that is changing the feed gas composition and finally affects drastically the measured ion composition.

For the interaction of cold atmospheric pressure plasmas with surfaces neutral particles dominate the flux and represent usually the main plasma-surface agent. To show that the effect of gas purification by the methods described above extends also to neutral species, the density of atomic nitrogen was investigated by molecular beam mass spectrometry (MBMS) and the results are shown in Fig. 6. The diagnostic details of MBMS and the method of calibration is explained in greater detail in [34] and the references therein.

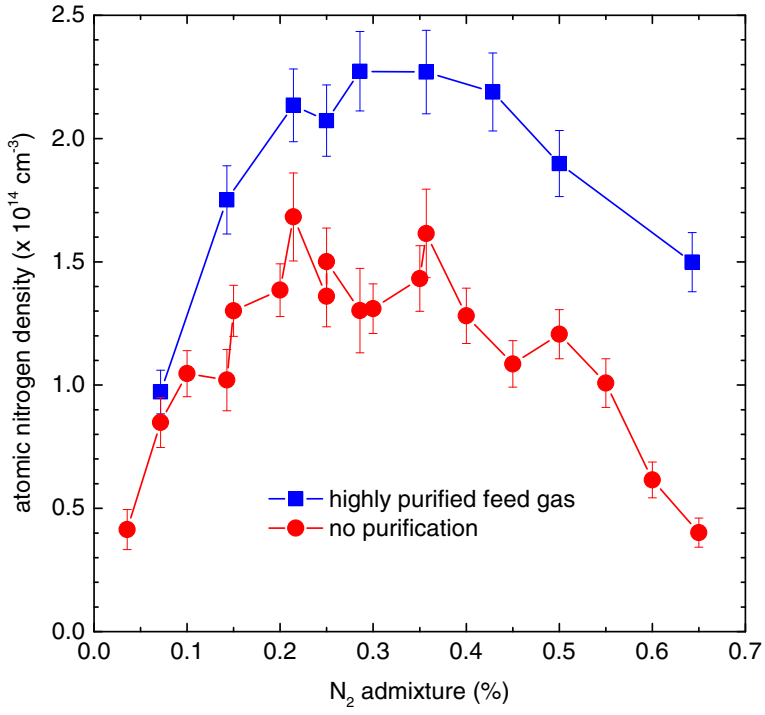

Fig. 6 Effect of purification by molecular sieve trap and liquid nitrogen trap on the density of atomic nitrogen in a μ-APPJ operated in 1.4 slm He with an variable admixture of N_2 measured by molecular beam mass spectrometry (MBMS) [34]

It should be noted that in this case the absorbed power at given voltage is influenced by the change in gas mixture. Higher nitrogen admixture reduces the absorbed power leading to the peculiar maximum of the atomic nitrogen density. However, the trends inside a specific figure in this study remain true, since the change due to purification is only a minor change in the absolute gas mixture and has consequently a minor influence on the absorbed power [35].

At an admixture of nitrogen of 0.25 % which is equal to the conditions used for the measurement shown above in Fig. 5, the density of N atoms increases by 50 % when the gas is purified. This can be attributed to the reduction of loss channels of primary nitrogen atoms and ions through reactions with H_2O and O_2 and its products. In [34] it was found that the afterglow density of N is significantly reduced by reactions such as $N + OH$ and $N + NO$.

Surprisingly, the relative density difference is the largest at the highest N_2 admixture used (0.65 %) and smaller at lower admixtures, where there should be relatively more impurities per N_2 molecule. First, the N density appears to be limited by its production rate proportional to the N_2 supply, and is not so much affected by impurities. However, as the N_2 admixture exceeds 0.25 % the saturation and decrease of the N density reveals that the N_2 dissociation rate is affected by the reduction of the absorbed power with higher N_2 percentage. This most likely causes a reduction of the electron density or maybe a change in the electron energy distribution function with respect to a pure He plasma. A plasma with lower ionization degree is consequently more sensitive to the presence of other molecular impurities. This shows that impurities even at small concentrations of the

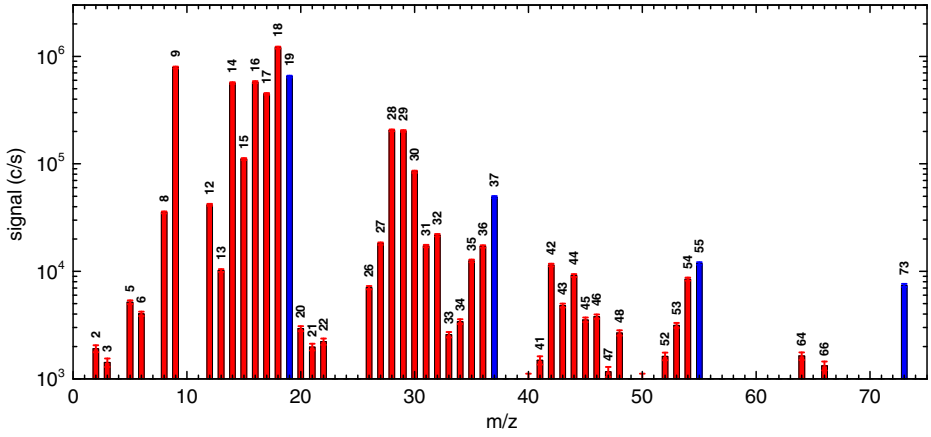

Fig. 7 Mass spectrum obtained from the μ-APPJ (0.7 slm He, $U_{rms} = 160\,\mathrm{V}$, $d = 2\,\mathrm{mm}$) operated in a controlled atmosphere. Possible ion assignments are presented in Table 1

order of a few ppm do not only significantly effect the ion- but also the neutral-chemistry in an atmospheric pressure plasma jet.

Analysis of the ion chemistry and kinetics

In the μ-APPJ operated in Helium increasing the purity of the feed gas generally leads to an unstable plasma. The plasma switches to a contracted γ-like mode with a high density plasma localized at the surface of the electrodes that results in their damage. Therefore, the standard operating conditions are modified by reducing the Helium flow to 0.7 slm and the applied voltage to $U_{rms} = 160\,\mathrm{V}$, which is close to the minimum voltage necessary for ignition and low enough to keep the plasma operating in an α-mode. These modifications enable to study a 'pure' helium plasma without the intentional admixture of reactive gases while using all above mentioned purification methods in situ. A simplified positive ion mass spectrum measured at a distance of $d = 2\,\mathrm{mm}$ is shown in Fig. 7. For each mass the maximum value is determined and the mass spectrum is shown as a bar chart. Negative ions are not observable which is attributed to the low amount of electronegative species and the high rates for ion-ion recombination ($\sim 10^{-13}\,\mathrm{m^3 s^{-1}}$ [36]) in the effluent before sampling.

As already shown in Fig. 3, a better gas purity enhances the appearance of lower mass ions. Even He_2^+ at $m/z = 8$ and maybe He_3^+ at $m/z = 12$ as primary ions from the plasma are observable. The direct neighboring signals with mass +1 are usually related to protonated species, e.g. HHe_2^+ at $m/z = 9$, HN^+ at $m/z = 15$ or HN_2^+ at $m/z = 29$. Such protonated neighbor signals appear for almost all main ion signals observable and underline the importance of proton transfer reactions. A list of possible ions corresponding to signals at specific m/z values with high abundance is shown in Table 1. For the sake of completeness also ions containing carbon are listed. However, the low expected content of CO_2 resulting from feed gas impurities and the use of oil-free pumps allows us to assume that C-containing ions do not contribute here.

Signals corresponding to molecular and atomic ions originating from impurities such as N_2^+, N^+, O_2^+, O^+ are observable. Such ions may be formed as primary ions inside

Table 1 Possible ions corresponding to most abundant signals shown in Fig. 7

m/z	He,H	N,H	O,H	N,O,H	C-containing
5	HHe^+				
8	He_2^+				
9	HHe_2^+				
12	He_3^+				C^+
14		N^+			CH_2^+
15		NH^+			CH_3^+
16	He_4^+	NH_2^+	O^+		CH_4^+
17	HHe_4^+	NH_3^+	OH^+		
18		NH_4^+	H_2O^+		
19			H_3O^+		
27					$C_2H_3^+$, HCN^+
28		N_2^+			$C_2H_4^+$, CO^+
29		HN_2^+			$C_2H_5^+$
30		$H_2N_2^+$		NO^+	$C_2H_6^+$, COH_2^+
31				HNO^+	
32			O_2^+	$N^+(H_2O)$	
34			$H_2O_2^+$		
37			$H^+(H_2O)_2$		
42		N_3^+			
44				N_2O^+	CO_2^+
46				NO_2^+,$N_2^+(H_2O)$	
48			O_3^+	$NO^+(H_2O)$	
55			$H^+(H_2O)_3$		
64				$N_2^+(H_2O)_2$	
66				$NO^+(H_2O)_2$	
73			$H^+(H_2O)_4$		

the plasma through electron impact ionization, dissociative ionization as well as Penning ionization by helium metastables. The high collision rate at atmospheric pressure leads to modifications of this primary ion composition due to charge transfer, attachment and proton transfer reactions as well as cluster formation resulting in the appearance of $H^+(H_2O)_n$ and $NO^+(H_2O)_n$. With increasing distance to the sampling orifice the number of collisions and thereby the probability of charge transfer and proton transfer reactions is increasing. Changes of the ion composition are expected and were found in a distance variation while measuring a full mass spectrum at each position. The signal as a function of the distance of selected ions is shown in Fig. 8.

In Fig. 8(a) signals corresponding to non-water ions are summarized while in Fig. 8(b) the distance dependence of water cluster ions is shown. A steep exponential signal reduction is observable for ions with low mass such as He_2^+, HHe_2^+, N^+, O^+. Such species are only detectable up to a maximum distance of 5 mm. These ions are primary ions or are created inside the plasma zone and survive the transport from the exit of the jet to the sampling orifice as long as the distance and the corresponding number of collisions is small enough.

By analysis of the dominant reaction rates, the reaction pathway can be identified. We assume the largest impurity concentration being N_2 followed by water. $[N_2] \approx 3 \times 10^{-6}\, n_{He}$ (3 ppm) according to the manufacturer's specification, the water concentration

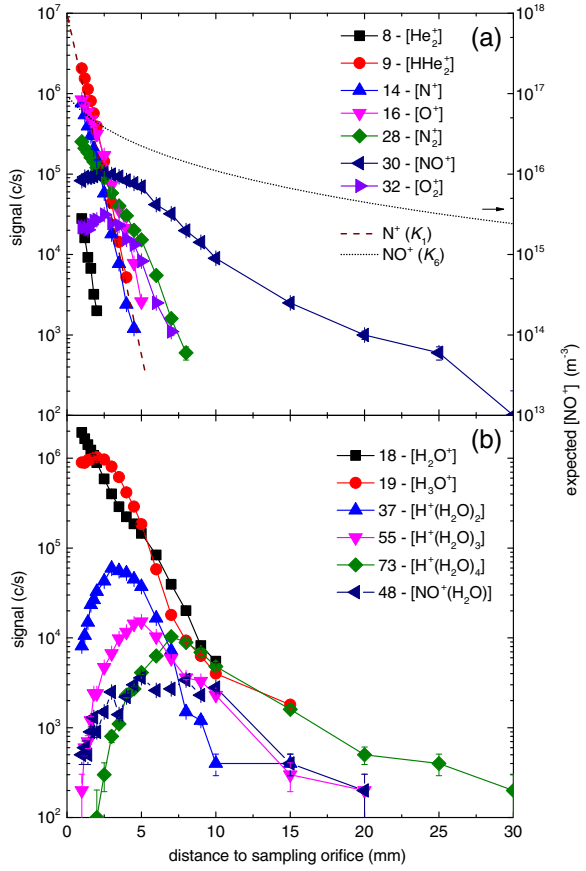

Fig. 8 Selected ion signals from μ-APPJ (0.7 slm He, $U_{rms} = 160$ V, $d = 2$ mm) in dependence on the distance to the sampling orifice orifice. The assignments in square brackets are corresponding to the most likely ion. For clarity the ions are separated into to groups summarizing (**a**) non-water and (**b**) water-containing ions. The dashed lines show the expected trends for N^+ and NO^+ based on reactions (4) and (10), respectively

can only be estimated to be around 0.1 ppm based on the reduction seen in Fig. 6. The lighter ions decay rapidly by means of attachment reactions such as

$$K_1\left(\mathrm{N}^+ + \mathrm{N}_2 + \mathrm{M} \rightarrow \mathrm{N}_3^+ + \mathrm{M}\right) = n_{\mathrm{He}} k_1 \approx 1.2 \times 10^{-15}\,\mathrm{m}^3\mathrm{s}^{-1}\ [37] \quad (4)$$

$$K_2\left(\mathrm{O}^+ + \mathrm{N}_2 + \mathrm{M} \rightarrow \mathrm{N} + \mathrm{NO}^+ + \mathrm{M}\right) = n_{\mathrm{He}} k_2 \approx 1.5 \times 10^{-15}\,\mathrm{m}^3\mathrm{s}^{-1}\ [38] \quad (5)$$

$$K_3\left(\mathrm{N}_2^+ + \mathrm{N}_2 + \mathrm{M} \rightarrow \mathrm{N}_4^+ + \mathrm{M}\right) = n_{\mathrm{He}} k_3 \approx 1.3 \times 10^{-15}\,\mathrm{m}^3\mathrm{s}^{-1}\ [38]. \quad (6)$$

Charge transfer reaction to water have even larger rate constants, but the lower water abundance leads to slower decay rates. For the He ions the charge transfer reactions to N_2 are most favorable

$$K_4(\mathrm{He}^+ + \mathrm{N}_2 \rightarrow \mathrm{He} + \mathrm{products}) = k_4 \approx 1.2 \times 10^{-15}\,\mathrm{m}^3\mathrm{s}^{-1} \quad (7)$$
$$[38], \text{B011+B012 in } [39]$$

$$K_5(\mathrm{He}_2^+ + \mathrm{N}_2 \rightarrow \mathrm{N}_2^+ + \mathrm{products}) = k_5 \approx 2.6 \times 10^{-15}\,\mathrm{m}^3\mathrm{s}^{-1} \quad (8)$$
$$[38], \text{B025+B026 in } [39].$$

Together with the mentioned impurity densities, the effective reaction rate coefficients K_1 to K_5 give lifetimes between $\tau_{K_1,K_4} \approx 11$ μ s and $\tau_{K_5} \approx 5$ μ s. These calculated lifetimes

can be compared with measured decay times of individual ions. For example N^+ decays by one order of magnitude in 25 μ s for a gas velocity of 23 m/s at the jet exit. This can be converted in an experimental lifetime

$$\tau_{\text{exp}} = \frac{25\,\mu\text{s}}{\ln(10)} \approx 11\,\mu\text{s}. \tag{9}$$

which matches very well the lifetime for reaction (4) $\tau_{K_1} \approx 11\mu$ s. This is equivalent to the dashed straight line interpolating the N^+ ion decrease as a function of distance to sampling orifice in Fig. 8(a) assuming an exponential decay with an arbitrary offset.

The signal corresponding to N_2^+ also shows a steep exponential decay up to a distance of 5 mm. However, at this point the decay rate changes and the signal is dropping more rapidly than before until it is not detectable any more at a distance of 8 mm from the sampling orifice. This change of the rate of ion depletion might be related to the loss of the lighter ions up to a distance of 5 mm. At this point such ions are not available any more as a precursor for possible charge-transfer reactions resulting in a reduced formation of N_2^+ that finally appears as an increased depletion.

Eventually secondary or terminal ions appear that exhibit a different decay behavior. The NO^+ ion at $m/z = 30$ is a prominent example of this decay behavior when looking at the corresponding distance curve. The signal increases until it peaks at 2 mm and slowly decreases at larger distances. The signal is measurable up to a distance of more than 20 mm in contrast to the lighter ions discussed so far. This observation is explained by the low ionization energy of the neutral NO of only 9.26 eV. This low ionization energy favors NO^+ as a terminal ion in a chain of exothermic charge transfer reactions. The trend of NO^+ is apparently governed by at least two mechanisms; a production and a loss channel. The first is either formation of NO^+ by attachment or charge transfer to NO and the loss channel in the late afterglow by recombination or ion clustering. Further charge transfer is very unlikely in this gas mixture. The dissociative recombination rate for the long-living NO^+ is

$$K_6(\text{e} + \text{NO}^+ -> \text{N} + \text{O}) = k_6 \approx 4.3 \times 10^{-13}\,\text{m}^3\text{s}^{-1}[40] \tag{10}$$

for thermalized electrons at 300 K. The trend of reaction (10) is indicated by the dotted line in Fig. 8(a), assuming a charge density of $n_e \approx 10^{17}$ m^{-3} [28] (right scale with same number of decades). The calculated decay is too slow compared to the experimental decay curve of NO^+, but the message here is to show that the density is ruled by recombination and not charge transfer as in the early afterglow. The $NO^+(H_2O)$ cluster ion is formed due to associative reaction of NO^+ with H_2O, which presents another important loss channel of NO^+ and could indeed explain the difference, however, we refrain from more detailed kinetic modeling as this exceeds the scope of the paper. Moreover, in this simple picture we did not account for negative-positive ion recombination, as the mass spectra indicates no negative ions, nor for diffusive and advective losses of ions. Eventually, misalignment of the sampling orifice normal and the effluent axis could occur.

The water cluster ions show similar trends summarized in Fig. 8(b). While the pure water ion H_2O^+ shows a clear exponential decay, all heavier cluster ions $H^+(H_2O)_n$ with $n \geq 1$ show a peak at a specific distance from the sampling orifice. The location of the peak is increasing with increasing cluster ion mass, i.e. 2 mm for $n = 1$, 3 mm for $n = 2$, 5 mm for $n = 3$, and 7 mm for $n = 4$. The mechanism of water cluster ion formation was explained in the previous section in Eqs. 1–3. Starting with H_2O^+ as a primary ion

formed in the plasma by electron impact or Penning ionization, it is converted to H_3O^+ by reactions with neutral water molecules. In the next step, the loss channel of the newly formed H_3O^+ is given by the formation of heavier cluster ions such as $H^+(H_2O)_2$ which wins against the production rate at a certain distance corresponding to a specific number of collisions. Since each water cluster ion is a precursor for the next heavier water cluster ion, this process propagates with increasing distance resulting in the observation of the peak appearing at a larger distance with increasing cluster size.

Conclusions

The ion chemistry of a radio-frequency driven atmospheric pressure plasma jet (μ-APPJ) operated in Helium in a controlled and well-defined atmosphere has been investigated using ion mass spectrometry. Without careful purification of the feed gas helium (5.0) the mass spectrum is dominated by water cluster ions $H^+(H_2O)_n$ with $n = 1 \ldots 5$. Feed gas purification was successfully achieved by using stainless steel tubes for gas transport, a molecular sieve trap and a liquid nitrogen trap. By this the content of impurities could be reduced significantly by about two orders of magnitude, indicating a residual concentration of oxygen-containing species of less than 0.1 ppm. However, even at such a low level of impurities the ion chemistry in the effluent of the μ-APPJ operated without additional admixture of reactive gases is dominated by impurities.

Summarizing, it is concluded that from a cold plasma at atmospheric pressure no *clean* helium ion spectra can be expected. Ions originating from nitrogen, oxygen and water are dominating the mass spectrum, because of the strong tendency of ion conversion and Penning reaction by the highly energetic He metastable species. This can be extrapolated for the ion chemistry of plasmas operated in pure noble gases (He, Ne and to some extend Ar) which are dominated by impurities as shown by the results presented here. The measured ion spectrum as a function of the distance identifies primary and secondary ions. Especially for plasmas close-by or in direct contact with a treatment area this difference might be very important and can be used accordingly for instance to achieve the appropriate soft ionization of a target or analyte. Moreover, not only the ion chemistry but also the neutral composition is changed by the cleaning as well, which was shown for a μ-APPJ operated in a Helium-nitrogen mixture and analyzed by molecular beam mass spectrometry (MBMS).

Acknowledgements
This work has been funded by the German Research Foundation (DFG, grant PlasmaDecon PAK 728 to Jan Benedikt (BE 4349/2-1)), as well as FOR 1123 and the Research Department Plasmas with Complex Interactions of the Ruhr-University Bochum (RUB) and the Marie Curie international training network 'RAPID'. The authors would like to thank Norbert Grabkowski for his technical support and S. Matejčík for the helpful discussions.

Authors' contributions
SGK designed and build the set-up under supervision of AvK and JB. JB proposed the purification steps which SiS and SGK prepared. SGK and SH conducted the experiment. SGK and SH wrote the manuscript while SH, SiS, JB and AvK revised it. All authors read and approved the final manuscript.

Competing interests
The authors declare that they have no competing interests.

Received: 4 May 2016 Accepted: 17 August 2016
Published online: 02 September 2016

References

1. Iza F, Kim GJ, Lee SM, Lee JK, Walsh JL, Zhang YT, Kong MG. Microplasmas: Sources, particle kinetics, and biomedical applications. Plasma Process Polym. 2008;5(4):322–344. doi:10.1002/ppap.200700162. Accessed 10 Oct 2014.

2. Miclea M, Kunze K, Franzke J, Niemax K. Microplasma jet mass spectrometry of halogenated organic compounds. J Anal At Spectrom. 2004;19(8):990. doi:10.1039/b401319k.
3. Guaitella O, Sobota A. The impingement of a khz helium atmospheric pressure plasma jet on a dielectric surface. J Phys D Appl Phys. 2015;48(25):255202. doi:10.1088/0022-3727/48/25/255202.
4. Gathen VS-vd, Schaper L, Knake N, Reuter S, Niemi K, Gans T, Winter J. Spatially resolved diagnostics on a microscale atmospheric pressure plasma jet. J Phys D Appl Phys. 2008;41(19):194004. doi:10.1088/0022-3727/41/19/194004.
5. Massines F, Gherardi N, Fornelli A, Martin S. Atmospheric pressure plasma deposition of thin films by townsend dielectric barrier discharge. Surf Coat Technol. 2005;200(5–6):1855–1861. doi:10.1016/j.surfcoat.2005.08.010.
6. Premkumar PA, Starostin SA, Creatore M, Vries Hd, Paffen RMJ, Koenraad PM, van de Sanden, MCM. Smooth and self-similar sio2-like films on polymers synthesized in roll-to-roll atmospheric pressure-pecvd for gas diffusion barrier applications. Plasma Process Polym. 2010;7(8):635–639. doi:10.1002/ppap.200900179.
7. Rügner K, Reuter R, Keudell Av, Benedikt J. The effect of surface reactions of o, o 3 and n on film properties during the growth of silica-like films. J Phys D Appl Phys. 2014;47(22):224005. doi:10.1088/0022-3727/47/22/224005.
8. Beck AJ, Aranda Gonzalvo Y, Pilkington A, Yerokhin A, Matthews A. Positive ion mass spectrometry during an atmospheric pressure plasma treatment of polymers. Plasma Process Polym. 2009;6(8):521–529. doi:10.1002/ppap.200800220.
9. Noeske M, Degenhardt J, Strudthoff S, Lommatzsch U. Plasma jet treatment of five polymers at atmospheric pressure: surface modifications and the relevance for adhesion. Int J Adhes Adhes. 2004;24(2):171–177. doi:10.1016/j.ijadhadh.2003.09.006.
10. Borris J, Dohse A, Hinze A, Thomas M, Klages CP, Möbius A, Elbick D, Weidlich ER. Improvement of the adhesion of a galvanic metallization of polymers by surface functionalization using dielectric barrier discharges at atmospheric pressure. Plasma Process Polym. 2009;6(S1):258–263. doi:10.1002/ppap.200930606.
11. Isbary G, Stolz W, Shimizu T, Monetti R, Bunk W, Schmidt HU, Morfill GE, Klämpfl TG, Steffes B, Thomas HM, Heinlin J, Karrer S, Landthaler M, Zimmermann JL. Cold atmospheric argon plasma treatment may accelerate wound healing in chronic wounds: Results of an open retrospective randomized controlled study in vivo. Clin Plasma Med. 2013;1(2):25–30. doi:10.1016/j.cpme.2013.06.001.
12. Kong MG, Kroesen G, Morfill G, Nosenko T, Shimizu T, van Dijk J, Zimmermann JL. Plasma medicine: an introductory review. New J Phys. 2009;11(11):115012. doi:10.1088/1367-2630/11/11/115012.
13. Dobrynin D, Fridman G, Friedman G, Fridman A. Physical and biological mechanisms of direct plasma interaction with living tissue. New J Phys. 2009;11(11):115020. doi:10.1088/1367-2630/11/11/115020.
14. Dobrynin D, Friedman G, Fridman A, Starikovskiy A. Inactivation of bacteria using dc corona discharge: role of ions and humidity. New J Phys. 2011;13:. doi:10.1088/1367-2630/13/10/103033.
15. Blake RS, Monks PS, Ellis AM. Proton-transfer reaction mass spectrometry. Chem Rev. 2009;109(3):861–96. doi:10.1021/cr800364q.
16. Große-Kreul S, Hübner S, Schneider S, Ellerweg D, Keudell Av, Matejčík S, Benedikt J. Mass spectrometry of atmospheric pressure plasmas. Plasma Sources Sci Technol. 2015;24(4):044008. doi:10.1088/0963-0252/24/4/044008.
17. Barnett RN, Landman U. Structure and energetics of ionized water clusters: (h2o)n+, n=2–5. J Phys Chem A. 1997;101:164–169.
18. Bruggeman P, Iza F, Lauwers D, Gonzalvo YA. Mass spectrometry study of positive and negative ions in a capacitively coupled atmospheric pressure rf excited glow discharge in he–water mixtures. J Phys D Appl Phys. 2010;43(1):012003. doi:10.1088/0022-3727/43/1/012003.
19. Skalny JD, Orszagh J, Mason NJ, Rees JA, Aranda-Gonzalvo Y, Whitmore TD. Mass spectrometric study of negative ions extracted from point to plane negative corona discharge in ambient air at atmospheric pressure. Int J Mass Spectrom. 2008;272(1):12–21. doi:10.1016/j.ijms.2007.12.012.
20. Oh JS, Aranda-Gonzalvo Y, Bradley JW. Time-resolved mass spectroscopic studies of an atmospheric-pressure helium microplasma jet. J Phys D Appl Phys. 2011;44(36):365202. doi:10.1088/0022-3727/44/36/365202.
21. McKay K, Walsh JL, Bradley JW. Observations of ionic species produced in an atmospheric pressure pulse-modulated rf plasma needle. Plasma Sources Sci Technol. 2013;22(3):035005. doi:10.1088/0963-0252/22/3/035005.
22. McKay K, Oh JS, Walsh JL, Bradley JW. Mass spectrometric diagnosis of an atmospheric pressure helium microplasma jet. J Phys D Appl Phys. 2013;46(46):464018. doi:10.1088/0022-3727/46/46/464018.
23. Malović G, Puač N, Lazović S, Petrović Z. Mass analysis of an atmospheric pressure plasma needle discharge. Plasma Sources Sci Technol. 2010;19(3):034014. doi:10.1088/0963-0252/19/3/034014.
24. Niermann B, Kanitz A, Böke M, Winter J. Impurity intrusion in radio-frequency micro-plasma jets operated in ambient air. J Phys D Appl Phys. 2011;44(32):325201. doi:10.1088/0022-3727/44/32/325201.
25. Winter J, Wende K, Masur K, Iseni S, Dünnbier M, Hammer MU, Tresp H, Weltmann KD, Reuter S. Feed gas humidity: a vital parameter affecting a cold atmospheric-pressure plasma jet and plasma-treated human skin cells. J Phys D Appl Phys. 2013;46(29):295401. doi:10.1088/0022-3727/46/29/295401.
26. Knake N, Schröder D, Winter J, Gathen VS-Vd. Investigations on the generation of atomic oxygen inside a capacitively coupled atmospheric pressure plasma jet. J Phys Conf Ser. 2010;227:012020. doi:10.1088/1742-6596/227/1/012020.
27. Niermann B, Hemke T, Babaeva NY, Böke M, Kushner MJ, Mussenbrock T, Winter J. Spatial dynamics of helium metastables in sheath or bulk dominated rf micro-plasma jets. J Phys D Appl Phys. 2011;44(48):485204. doi:10.1088/0022-3727/44/48/485204.
28. Waskoenig J, Niemi K, Knake N, Graham LM, Reuter S, Gathen VS-Vd, Gans T. Atomic oxygen formation in a radio-frequency driven micro-atmospheric pressure plasma jet. Plasma Sources Sci Technol. 2010;19(4):045018. doi:10.1088/0963-0252/19/4/045018.
29. Schneider S, Lackmann JW, Ellerweg D, Denis B, Narberhaus F, Bandow JE, Benedikt J. The role of vuv radiation in the inactivation of bacteria with an atmospheric pressure plasma jet. Plasma Process Polym. 2012;9(6):561–568. doi:10.1002/ppap.201100102.
30. Golda J, Held J, Redeker B, Konkowski M, Beijer P, Sobota A, Kroesen G, Braithwaite NSJ, Reuter S, Turner MM, Gans T, O'Connell D, der Gathen VS-Vd. Concepts and characteristics of the 'cost reference microplasma jet'. J Phys D Appl Phys. 2016;49(8):084003.

31. Schütze A, Jeong YJ, Babayan SE, Park J, Selwyn GS, Hicks RF. The atmospheric-pressure plasma jet: a review and comparison to other plasma sources - plasma science, ieee transactions on. IEEE Trans Plasma Sci. 1998;26(6): 1685–1694.
32. Müller IB, Cederbaum LS. Ionization and double ionization of small water clusters. J Chem Phys. 2006;125(20): 204305. doi:10.1063/1.2357921.
33. Schneider S, Jarzina F, Lackmann JW, Golda J, Layes V, der Gathen VS-Vd, Bandow JE, Benedikt J. Summarizing results on the performance of a selective set of atmospheric plasma jets for separation of photons and reactive particles. J Phys D Appl Phys. 2015;48(44):444001.
34. Schneider S, Dünnbier M, Hübner S, Reuter S, Benedikt J. Atomic nitrogen: a parameter study of a micro-scale atmospheric pressure plasma jet by means of molecular beam mass spectrometry. J Phys D Appl Phys. 2014;47(50): 505203. doi:10.1088/0022-3727/47/50/505203. Accessed 12 Feb 2014.
35. Marinov D, Braithwaite NStJ. Power coupling and electrical characterization of a radio-frequency micro atmospheric pressure plasma jet. Plasma Sources Sci Technol. 2014;23(6):062005. doi:10.1088/0963-0252/23/6/062005.
36. Fridman A, Kennedy LA. Plasma Physics and Engineering. NY London: Taylor & Francis; 2004. https://books.google.de/books?id=9wqtYiy_gloC.
37. Märk TD, Oskam HJ. Ion production and loss processes in helium-nitrogen mixtures. Phys Rev A. 1971;4:1445–1452. doi:10.1103/PhysRevA.4.1445.
38. Bortner MH, Baurer T. Defense nuclear agency reaction rate handbook, second edition. Santa Barbara, California: General Electric, TEMPO; 1972.
39. Murakami T, Niemi K, Gans T, O'Connell D, Graham WG. Chemical kinetics and reactive species in atmospheric pressure helium–oxygen plasmas with humid-air impurities. Plasma Sources Sci Technol. 2013;22(1):015003. doi:10.1088/0963-0252/22/1/015003.
40. Mitchell JBA. The dissociative recombination of molecular ions. Phys Rep. 1990;186(5):215–248. doi:10.1016/0370-1573(90)90159-Y.